

Kinetics-Driven Growth of Orthogonally Branched Single-Crystalline Magnesium Oxide Nanostructures

Yufeng Hao, Guowen Meng,* Changhui Ye, Xueru Zhang, and Lide Zhang

Key Laboratory of Materials Physics, Institute of Solid State Physics, Chinese Academy of Sciences, Hefei, 230031, People's Republic of China

Received: February 1, 2005; In Final Form: April 14, 2005

Orthogonally branched single-crystalline magnesium oxide nanostructures were synthesized through a simple chemical vapor transport and condensation process in a flowing Ar/O₂ atmosphere. Other morphologies, such as cubes and nanowires, can also be obtained under different controlled conditions. The formation of different types of nanostructures can be tuned by modifying oxygen partial pressure during the synthesis. All the nanostructures are cubic single-crystalline enclosed by low-index {100} facets. Growth mechanisms for the nanostructures are discussed in detail: different supersaturation ratios, relatively high substrate temperatures, and surface defects in certain crystallographic planes cooperatively take important effects on determining the product morphologies. Structural defect-related blue light emission of the three types of MgO nanostructures was investigated. The MgO nanostructures with abundant morphologies may find applications in various nanodevices, and the kinetics-driven methodology might be exploited to synthesize similar nanostructures of other functional oxide materials.

Introduction

One-dimensional nanostructures (nanowires, nanobelts, nanotubes, etc.) will become prospective building blocks for various next generation nanodevices. Therefore, much effort has been devoted to this field.¹ However, effective assembly or interconnecting of these nanostructures to complex device systems remains a challenge. The fabrication of nanodevice systems by either self-assembly or improved Langmuir–Blodgett approach entails lengthy and elaborate processing although such advanced technologies have been adopted by several laboratories.² The newly developed hierarchical and branched nanostructures may represent an alternative toward the scaling up of the building blocks into functional devices. Ren et al. and Wang et al. have systematically explored the growth of hierarchical ZnO, In₂O₃, and SnO nanostructures, in which the core and the branches display a certain orientation relationship by chemical vapor deposition;³ as for the branched nanostructures, some progress has also been made: Samuelson et al.⁴ have synthesized GaP “nanotrees” with the assistance of Au aerogel through multistep vapor routes; Lieber et al.⁵ obtained branched and hyperbranched Si nanowires by similar methods. The common point about the branched nanowires is nucleation and growth dominated by the Vapor–Liquid–Solid (VLS) growth mechanism. This mode inevitably introduces heterometal impurity and affects their performance. As is well-known, the Vapor–Solid (VS) growth mechanism is another mode in the synthesis of one-dimensional nanostructures without metal impurity.^{6,7} However, the VS process without the steering of catalyst was an intractable technique since there are many external conditions and local circumstance fluctuation that affect the final morphologies of nanostructures. Furthermore, nanostructures, owing to their ultrasmall size, can exhibit distinct morphologies due to slight variation of growth conditions. In practical experiments, the aims are strengthening the effects of favored external parameters and

minimizing, or even avoiding obstructive ones. Therefore, overall understanding of crystallographic growth mechanisms and precise control of experimental parameters are critical to the synthesis of desired nanostructures.

Recently, various MgO nanostructures have been synthesized, such as nanorods,⁶ fishbone fractal nanostructures induced by Co,⁸ nanowires by oxide-assistant catalytic growth⁹ and by using MgB₂ precursors,¹⁰ nanobelts,^{11–13} nanotubes,¹⁴ Ga-filled MgO nanotubes,¹⁵ and three-dimensional entities.¹⁶ However, the controlled synthesis of several types of well-defined MgO nanostructures and specific growth mechanisms based on thermodynamics and kinetics are scarce.

In this article, three types of MgO nanostructures, i.e., orthogonally branched nanostructures, nanocubes (or microcubes), and straight nanowires, were achieved simply through heating magnesium (Mg) powders with different oxygen partial pressures. Detailed growth mechanisms for the three types of MgO nanostructures were discussed on the basis of the VS mode. Several growth conditions, especially oxygen partial pressures, play significant roles in determining the morphologies of the final products. Photoluminescence (PL) measurements reveal that these MgO nanostructures, especially orthogonally branched MgO nanostructures, have an intensive blue light emission band, suggesting potential applications in optoelectronic nanodevices.

Experimental Section

The synthesis of MgO nanostructures was carried out in a high-temperature horizontal tubular furnace. The local temperature distribution in the tubular furnace has been calibrated in advance. An alumina tube, 15 mm in inner diameter, was installed in the furnace. A ceramic boat loaded with Mg powders (99.99 wt %, 1 g) was inserted in the central heating zone of the alumina tube. Reaction time durations and temperatures are 10 min and 950 °C, respectively. Several silicon slices (100)

* Address correspondence to this author. E-mail: gwmeng@issp.ac.cn.

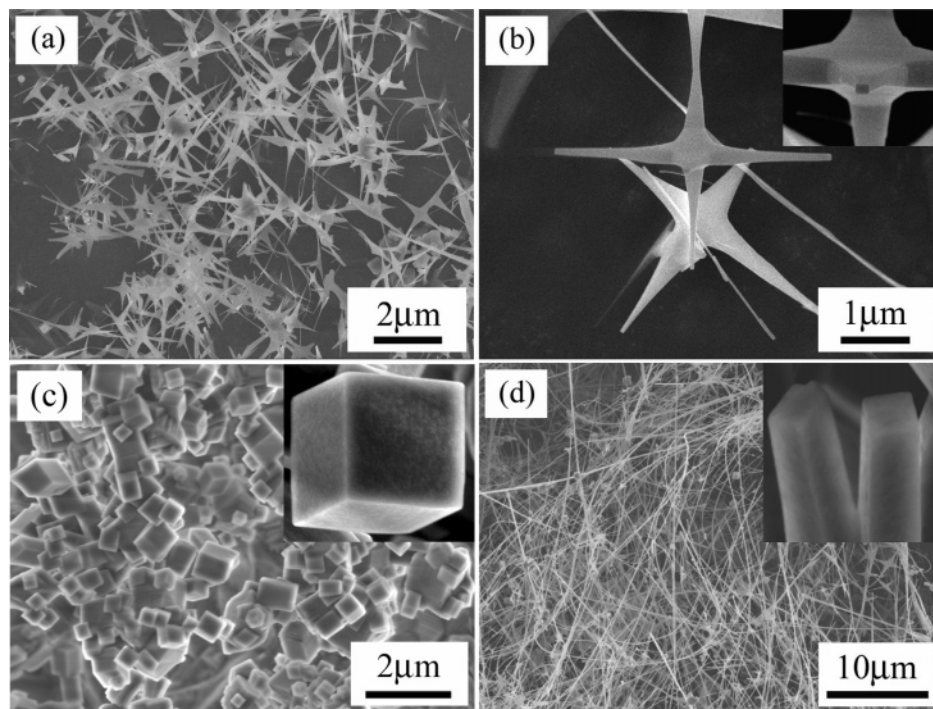


Figure 1. FESEM micrographs of the MgO nanostructures obtained at different oxygen partial pressures. (a, b) Low- and high-magnification images of branched nanostructures. The synthesis condition is 10% oxygen mixed in carrier Ar. The inset is the rectangle-shaped end of one branch. (c) MgO cubes, prepared with 4–5% oxygen mixed in Ar carrier gas; the inset is an enlarged image of a typical cube. (d) MgO nanowires, prepared with the lowest oxygen volume of 1–2% mixed in the carrier gas; the inset is a close-up view near the ends of the rectangle-shaped MgO nanowires

were placed downstream as deposition sites. During the whole process, high-purity argon (Ar) mixed with different volumes of high-purity oxygen (oxygen quantity ratio: 1–10%) was introduced into the reaction system as a carrier gas at 50 sccm. Different oxygen volume brings corresponding oxygen partial pressure. The products deposited on the Si slices, where the temperatures are about 850–900 °C, are wool-like or powder-like for different oxygen partial pressures.

The products obtained under different conditions were characterized by field emission scanning electron microscopy (FESEM JEOL, JSM6700F), transmission electron microscopy (TEM HITACHI H-800 at 200 kV), high-resolution TEM (HRTEM JEM2010 at 200 kV), and X-ray photoelectron spectroscopy (XPS, VG ESCALAB MKII). The optical properties of the products were investigated with a Edinburgh luminescence spectrometer FLS 920 (excitation source: Xe lamp).

Results and Characterizations

Branched nanostructures of MgO (Figure 1a) were obtained by adopting the highest oxygen volume of 10% mixed in Ar carrier gas. All the branches, with several micrometers long, radiate from their centers. A typical SEM view (Figure 1b) shows that the four adjacent branches are orthogonal to each other, and the diameter of each branch gradually decreases from several hundred to tens of nanometers along its growth direction. Another branch perpendicular to the image plane reveals its rectangular cross section in the inset of Figure 1b. Therefore, this branched nanostructure shows a 5- or 6-fold orthogonally branching morphology (the back branch cannot be viewed). Other orthogonally branched nanostructures, such as 3-fold and 4-fold, have also been observed. This is a common feature of the branched MgO nanostructures determined by cubic structural symmetry. Nearly perfect nanocubes and microcubes with

several hundred nanometers to the order of micrometers are formed under median oxygen partial pressure (oxygen volume ratio: 4–5%), as shown in Figure 1c. Six equivalent square facets are clearly exposed on the surface of each cube. Through further decreasing oxygen volume to 1–2%, straight and long MgO nanowires (Figure 1d) 30–150 nm in diameter and hundreds of micrometers in length were obtained. Similar to branched nanostructures, the cross sections of the long nanowires are also rectangular (inset of Figure 1d). No metal particle can be found at the ends of the nanowires. Further observation reveals that more than 90% of the structures in the final products are the desired nanostructures in each case. Therefore, morphology-controllability was achieved in our experiments.

TEM observations on the three types of nanostructures provide more detailed information. Panels a, b, and c in Figure 2 reveal 3- and 4-fold orthogonally branched nanostructures. The tapered branches have very fine tips with the diameters of the most fronts ~20 nm shown in Figure 2b. All the selected area electron diffraction (SAED, inset of each image) patterns taken from the central sites can be indexed to the reflection of the [100] zone axis. In fact, SAED patterns taken from every branch are essentially the same without tilting these specimens, implying the single-crystalline and homogeneous epitaxial crystallographic nature. TEM images of cubes and wires are shown in Figure 2, panels d and e, respectively, revealing flat side surfaces. Similar SAED patterns to those of the branched nanostructures suggest that cubes and wires are also enclosed by {100} facets. We can therefore conclude that the side surfaces of the nanowires are enclosed by $\pm(010)$ and $\pm(001)$ planes, and the front end is the (100) plane. In other words, the nanowires are prolonged nanocubes.

Two representative HRTEM images (Figure 3) of the MgO nanostructures show the expected (200) lattice fringes with interplanar spacing of 0.21 nm. For the branched nanostructures

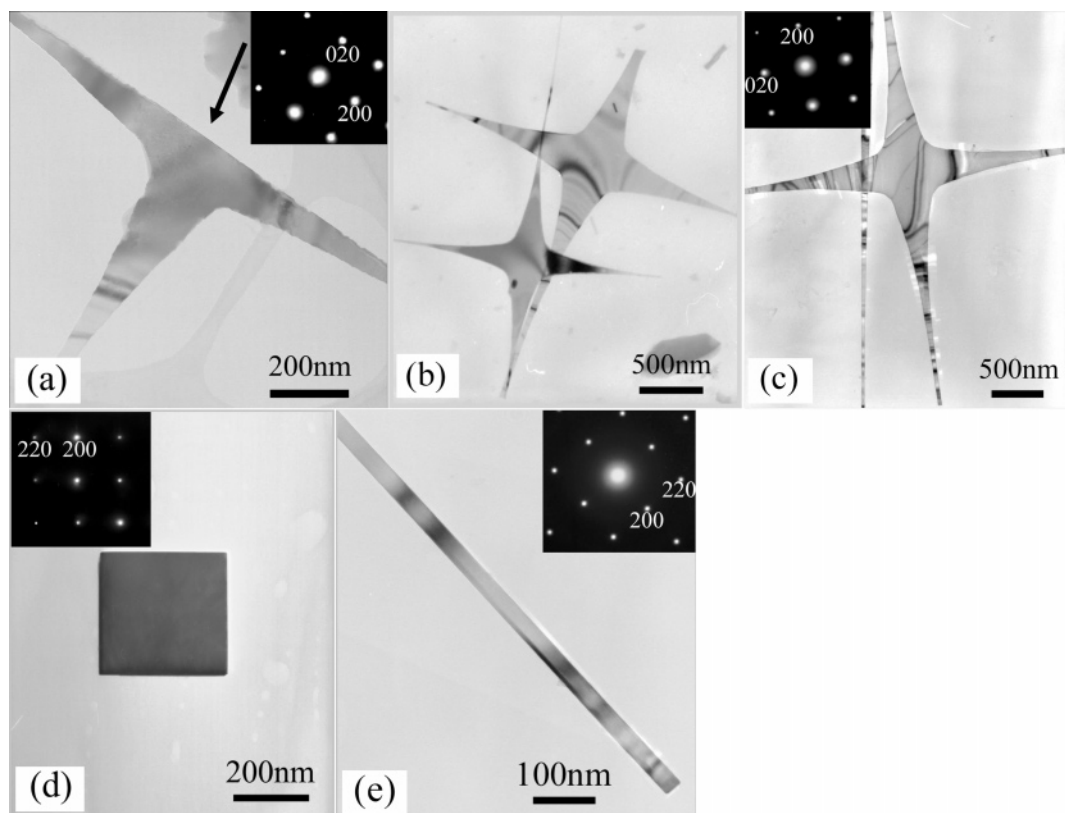


Figure 2. TEM images of orthogonally branched MgO nanostructures, cubes, and nanowires: (a) 3-fold branched nanostructures, (b, c) 4-fold branched nanostructures, (d) a single MgO cube, and (e) a single MgO nanowire. The insets are the corresponding SAED patterns.

(Figure 3a), the side surface reveals a series of “steps”, where only $\{100\}$ facets are exposed, demonstrating the origin of tapered branches, and low surface energies of $\{100\}$ facets. The lattice-resolved image from a single nanowire (Figure 3b) reveals the rough surface especially on the growth front. Various defects observed here imply the distinct situations of growth front in the growth process. The characteristics will be discussed in the following section.

The XPS spectrum (Figure S, Supporting Information) of the branched nanostructures shows two peaks at 530 and 49.5 eV, corresponding to the binding energy of O (1s) and Mg (2p) of MgO, respectively, which are very close to the standard values of bulk MgO. A weak peak around 285 eV corresponds to the C (1s) because slight contamination of the carbon element generally occurs on the specimen surface. No metal impurity trace can be found in the complete spectrum, confirming that the branched nanostructures are pure MgO.

Discussion of Growth Mechanism

In the last several years, various one-dimensional nanostructures, such as ZnO, ZnS, and SnO_2 , were successfully prepared through the VS process without introducing any heterometal catalysts.⁷ Generally, their growth directions are perpendicular to high surface energy planes, their cross sections are well-defined squares or rectangles, and their side surfaces are enclosed by certain low-index crystallographic planes to minimize the surface energy. However, MgO, possessing a cubic NaCl-type crystalline structure, is not extremely anisotropic. Nanowires, nanocubes, and branched nanostructures of MgO are enclosed by six equivalent low index $\pm(100)$, $\pm(010)$, and $\pm(001)$ planes. Therefore, the formation of the three types of nanostructures is considered to be driven by growth kinetics.¹⁷

During the high-temperature vapor reaction, Mg vapor was sufficiently oxidized to MgO clusters by oxygen. Therefore,

supersaturation ratios can be adjusted through changing oxygen partial pressures in Ar carrier gas. A detailed discussion follows.

MgO clusters are transported onto the Si substrate at the low-temperature zone, then deposit and nucleate. Considering the surface energy minimization, MgO nuclei may be close to cubic shape. Subsequently formed MgO clusters transported by carrier gas will be adsorbed on the surfaces of nuclei. Three activities about these adsorbed MgO clusters may occur:¹⁸ (1) desorption and evaporation directly or after migrating along the surface; (2) incorporation into the crystalline lattice at initial adsorption sites; and (3) surface diffusion and migration to high energy or high defect density sites and incorporation into crystalline lattice there. The probability among the three activities is affected by intrinsic structural characteristics and external controlled conditions. Brief schemes on the formation of the three types of MgO nanostructures are shown in Figure 4.

At low supersaturation ratio, the surface diffusion rate of newly arriving clusters is high, and the relatively high substrate temperatures around 850 °C guarantee that MgO clusters can migrate to high defect density sites (such as kinks, ledges, and steps) and incorporate into lattices there to minimize the surface energy.¹⁹ During the persistent growth, the high defect density surface will become the rough growth front, as demonstrated by the HRTEM image of one nanowire front end (Figure 3b). The other four planes will gradually turn to side surfaces. Therefore, nanowires of high aspect ratio are formed with $\langle 100 \rangle$ direction and enclosed by $\pm(010)$ and $\pm(001)$ planes. For the nearly perfect MgO crystal nuclei without necessary defects, however, the new cluster generally desorbs and evaporates even after surface diffusion because the supersaturation ratio is far below the required value for two-dimensional (2D) nucleation.¹⁹

With the increase of supersaturation ratio, more MgO clusters will arrive on the formed nuclei in the same time span. Thereby,

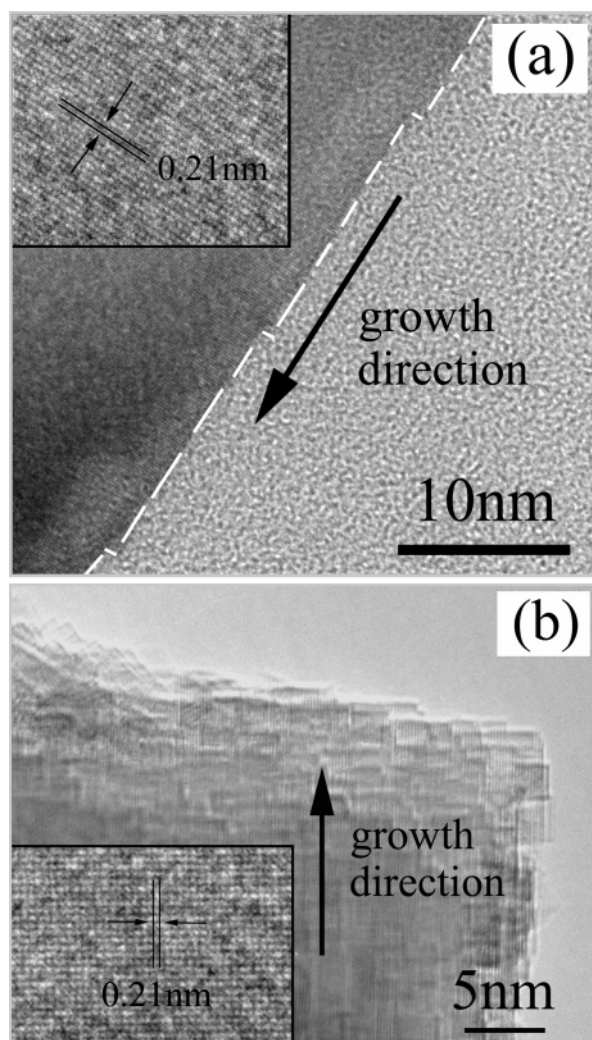


Figure 3. HRTEM images of MgO nanostructures: (a) a series of "steps" found on the side surface of a branched nanowire, with only {100} facets are exposed, and (b) the "rough" end of a straight nanowire. The insets are respective lattice-resolved images, revealing the spacing of (200) planes.

the probability of surface migration will decrease; correspondingly, 2D nucleation probability increases.²⁰ The growth rate of six equivalent (100) planes tends to be equal, which is close to thermodynamic equilibrium. Consequently, nanocubes and microcubes, the reflection of the crystalline structure of MgO, are formed.

Under further higher supersaturation ratios, a large quantity of clusters homogeneously adsorbs on the surfaces of cubic MgO nuclei. However, high defect density sites on each {100} facet of the nuclei incorporate more MgO clusters through surface diffusion and migration of these clusters and direct the growth of branches along the $\langle 100 \rangle$ direction. During the process, the most fronts of each branch dominate the growth owing to high defect density. Therefore, orthogonally branched nanostructures are formed in the form of homogeneous epitaxy. In addition, branches are shorter than straight MgO nanowires for a relatively short mean diffusion distance in the high supersaturation ratio (Figure 1a,d). Six-fold branched nanostructures are complete, but the appearance of other branched nanostructures, such as 3-fold, 4-fold, or 5-fold, originates from the great difference of the surface defect density on six (100) planes of MgO nuclei. As an example, a 3-fold branched nanostructure presented in Figure 2a should have a relatively low defect density on the upward plane (indicated by an arrowhead), which is difficult

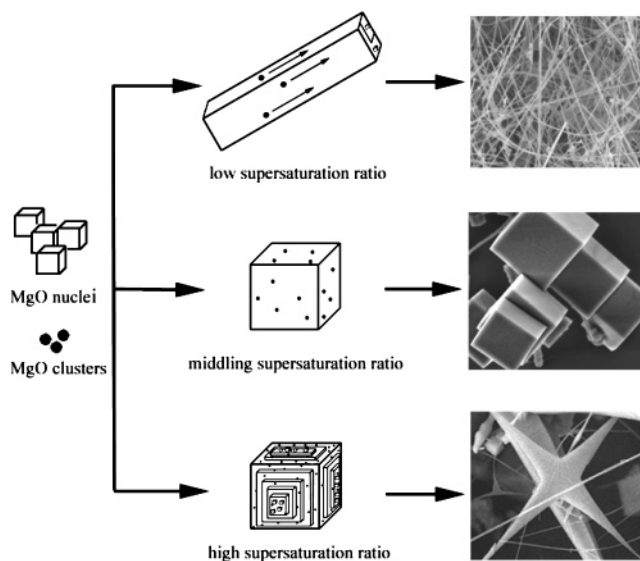


Figure 4. Schematic illustration of different MgO nanostructures formed under corresponding controlled conditions. The small black dots represent adsorbed MgO clusters.

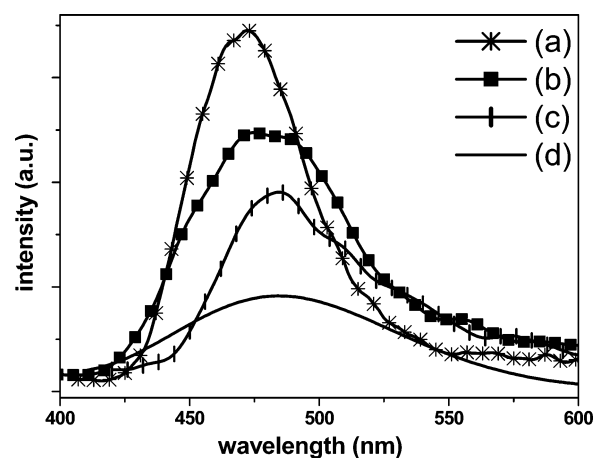


Figure 5. Room temperature PL spectra of MgO recorded under the same conditions: (a) for branched nanostructures, (b) for nanocubes, (c) for nanowires, and (d) for commercially available MgO powders.

for incorporation of MgO clusters into the crystalline lattice for continuous growth.

We mainly focus on the effect of oxygen partial pressures in determining the different morphologies of MgO nanostructures. Other external parameters, such as reaction temperatures, carrier gas flow rates, quantities of source materials, and alumina tube sizes, to some extent, will also affect the final morphologies. Further research on the effects and interaction of other growth conditions is underway.

Photoluminescence Properties

Optical investigations can reveal very useful information for understanding the physical properties of materials. Besides, through optical studies, it is possible to extend the potential application of MgO nanostructures in optoelectronic nano-devices. Room temperature PL spectra (Figure 5) of the as-prepared structures and commercially available MgO powders (purity: 99.99 wt %) were measured with an excitation wavelength of 380 nm in air. Compared with the weak and broad PL emission band of MgO powders, the PL of MgO nanostructures reveals strong bands with a peak position around 470 nm. Additionally, the branched nanostructures show more intensive

PL band than those of wires and cubes. It is evident that MgO nanostructures, especially orthogonally branched nanostructures, possess more unique optical properties than those of commercial powders. Clearly, the PL band is not the band gap emission, but can be attributed to various structural defects. For other MgO structures, Zhang et al.²¹ investigated PL characteristics of nanobelts and found PL bands around 383, 508, and 721 nm. Rosenblatt et al.²² reported the 390 and 530 nm bands in time-resolved PL spectra of bulk materials with different defect densities. In our experiments, rapid evaporation, incomplete oxidation, and crystallization may generate various structural defects, such as oxygen vacancy, which generally acts as deep defect donors in semiconductor oxide, and would induce the formation of new energy levels in the band gap of MgO. Therefore, the blue light emission may originate from the recombination of the photogenerated hole with an electron occupying the oxygen vacancy. Other possible defects, such as Mg vacancies and interstitials, may also contribute to the optical emission. The specific origin of the PL band broadening of the three types of MgO structures is not very clear. Different defect densities coming from corresponding growth conditions may be an important factor.

Conclusions

Orthogonally branched nanostructures, cubes, and straight nanowires of MgO induced by the VS growth mechanism were respectively synthesized by thermal evaporation of Mg in a gas mixture of Ar and O₂. Structural characterization reveals valuable information in understanding their growth mechanisms. Supersaturation ratios and surface defect density difference are two important factors in controlling the growth of various MgO nanostructures. Relatively high substrate temperatures are necessary to guarantee the diffusion and migration of MgO clusters. The blue light emission indicates potential application of the branched nanostructures in light emission devices. The discussion may have an important impact on the understanding of the physical and chemical process of the VS mode. Therefore, our methodology and experiments may promote the control of desired nanostructural morphologies of other functional oxide materials.

Acknowledgment. This work was supported by the Natural Science Foundation of China (Grant No. 10374092) and the Key Project of National Fundamental Research (973 Program,

Grant No. 1999064501). The authors thank Prof. Shuyuan Zhang, Prof. Jun Zhang, and Mr. Yongdong Yang for their technical assistance in HRTEM characterizations.

Supporting Information Available: Figure showing XPS spectra of the orthogonally branched MgO nanostructures: survey spectrum, Mg 2p spectrum, and O 1s spectrum. This material is available free of charge via the Internet at <http://pubs.acs.org>.

References and Notes

- (1) Xia, Y.; Yang, P.; Sun, Y.; Wu, Y.; Mayers, B.; Gates, B.; Yin, Y.; Kim, F.; Yan, H. *Adv. Mater.* **2003**, *15*, 353.
- (2) (a) Yang, P. *Nature* **2003**, *425*, 243. (b) Duan, X.; Niu, C.; Sahi, V.; Chen, J.; Parce, J. W.; Empedocles, S.; Goldman, J. L. *Nature* **2003**, *425*, 274. (c) Tao, A.; Kim, F.; Hess, C.; Goldberger, J.; He, R.; Sun, Y.; Xia, Y.; Yang, P. *Nano Lett.* **2003**, *3*, 1229. (d) Whang, D.; Jin, S.; Wu, Y.; Lieber, C. M. *Nano Lett.* **2003**, *3*, 1255.
- (3) (a) Gao, P. X.; Wang, Z. L. *J. Phys. Chem. B* **2002**, *106*, 12653. (b) Wang, Z. L.; Pan, Z. W. *Adv. Mater.* **2002**, *14*, 1029. (c) Lao, J. Y.; Huang, J. Y.; Wang, D. Z.; Ren, Z. F. *Nano Lett.* **2003**, *3*, 235. (d) Lao, J. Y.; Wen, J. G.; Wang, D. Z.; Ren, Z. F. *Int. J. Nanosci.* **2002**, *2*, 149. (e) Wen, J. G.; Lao, J. Y.; Wang, D. Z.; Kyaw, T. M.; Foo, Y. L.; Ren, Z. F. *Chem. Phys. Lett.* **2003**, *372*, 717.
- (4) Dick, K.; Deppert, K.; Larsson, M. W.; Martensson, T.; Seifert, W.; Wallenberg, L.; Samuelson, L. *Nat. Mater.* **2004**, *3*, 380.
- (5) Wang, D.; Qian, F.; Yang, C.; Zhong, Z.; Lieber, C. M. *Nano Lett.* **2004**, *4*, 871.
- (6) Yang, P. D.; Lieber, C. M. *J. Mater. Res.* **1997**, *12*, 2981.
- (7) Pan, Z. W.; Dai, Z. R.; Wang, Z. L. *Science* **2001**, *291*, 1947.
- (8) Zhu, Y. Q.; Hsu, W. K.; Zhou, W. Z.; Terrones, M. H.; Kroto, W.; Walton, D. R. M. *Chem. Phys. Lett.* **2001**, *347*, 337.
- (9) Tang, C. C.; Bando, Y.; Sato, T. *J. Phys. Chem. B* **2002**, *106*, 7449.
- (10) Yin, Y. D.; Zhang, G. T.; Xia, Y. N. *Adv. Funct. Mater.* **2002**, *12*, 293.
- (11) Li, Y.; Bando, Y.; Sato, T. *Chem. Phys. Lett.* **2002**, *359*, 141.
- (12) Ma, R.; Bando, Y. *Chem. Phys. Lett.* **2003**, *370*, 770.
- (13) Zhang, J.; Zhang, L.; Peng, X.; Wang, X. *Appl. Phys. A* **2001**, *73*, 773.
- (14) Zhan, J. H.; Bando, Y.; Hu, J. Q.; Golberg, D. *Inorg. Chem.* **2004**, *43*, 2462.
- (15) Li, Y. B.; Bando, Y.; Golberg, D.; Liu, Z. W. *Appl. Phys. Lett.* **2003**, *83*, 999.
- (16) Klug, K. L.; Dravid, V. P. *Appl. Phys. Lett.* **2002**, *81*, 1687.
- (17) Dai, Z. R.; Pan, Z. W.; Wang, Z. L. *Adv. Funct. Mater.* **2003**, *13*, 9.
- (18) Mullin, J. W. *Crystallization*, 3rd ed.; Butterworth-Heinemann: Oxford, UK, 1993.
- (19) Sears, G. W. *Acta Metall.* **1955**, *4*, 361.
- (20) Sears, G. W. *Acta Metall.* **1955**, *4*, 367.
- (21) Zhang, J.; Zhang, L. *Chem. Phys. Lett.* **2002**, *363*, 293.
- (22) Rosenblatt, G. H.; Rowe, M. W.; Williams, G. P., Jr.; Williams, R. T.; Chen, Y. *Phys. Rev. B* **1989**, *39*, 10309.